論文 / 著書情報
Article / Book Information

Title	Fracture Energy Determination of Wedge-opening Double Cantilever Beam Tests
Authors	Keiyu Ikeda, Yu Sekiguchi, Kazumasa Shimamoto, Chiaki Sato
Citation	The Journal of Adhesion, Vol. 101, pp. 1143-1162
Pub. date	2024, 11
Creative Commons	See next page.

License

THE JOURNAL OF ADHESION
2025, VOL. 101, NO. 9, 1143–1162
https://doi.org/10.1080/00218464.2024.2429406

Taylor & Francis
Taylor & Francis Group

Fracture Energy Determination of Wedge-opening Double Cantilever Beam Tests

Keiyu Ikeda[a], Yu Sekiguchi[b], Kazumasa Shimamoto[c], and Chiaki Sato[b]

[a]Department of Mechanical Engineering, Tokyo Institute of Technology, Yokohama, Japan; [b]Institute of Innovative Research (IIR), Tokyo Institute of Technology, Yokohama, Japan; [c]Nanomaterials Research Institute, National Institute of Advanced Industrial Science and Technology (AIST), Tsukuba, Japan

ABSTRACT

Adhesive fracture energy is often measured using the double cantilever beam (DCB) test method. However, opening a DCB specimen using a wedge differs the direction of the applied load from that of standard methods. The additional moment due to the longitudinal load alters the load-displacement-crack length relationship, requiring modifications in fracture energy calculation. The energy release rate (ERR) approach and the J-integral approach have been proposed to evaluate the fracture energy in wedge-opening DCB tests. However, these theories have limitations regarding wedge angles. In this study, we extended these theories to accommodate arbitrary wedge angles and performed numerical analyses to evaluate the accuracy of the theories. When the additional moment effect is neglected, the more obtuse the wedge angle and the thinner the adherend, the greater the error in the ERR. The error was over 5% when the wedge angle exceeded 90°. However, using the proposed ERR method, the error was reduced to less than 2% for all the wedge angles. When pin blocks were introduced into the DCB specimen, the additional moment effects increased the error to more than 5% even using the proposed ERR method. In this case, the modified J integral method yielded the lowest error results.

ARTICLE HISTORY
Received 26 August 2024
Accepted 5 November 2024

KEYWORDS
cohesive zone model; Fracture toughness; finite element method; impact DCB test; linear elastic fracture mechanics

1. Introduction

The demand for adhesive bonding as a structural joint continues to increase in several industries, such as automotive, aircraft, and marine.[1] Adhesive bonding offers advantages over other joining methods when joining dissimilar materials, designing lightweight products, or improving vibration absorption. Joints must transfer large loads for structural use; therefore, reliability is a primary factor. Accurate prediction of strength is essential in the joint design of structural parts, and numerical analysis using the finite element method (FEM) is considered an effective method for strength evaluation. In particular, when analyzing fractures involving crack propagation in FEM, the cohesive

CONTACT Keiyu Ikeda ikeda.k.bi@m.titech.ac.jp Department of Mechanical Engineering, Tokyo Institute of Technology, 4259 Nagatsuta-Cho, Midori-Ku, Yokohama 226-8501, Japan

zone model (CZM) has been widely adopted for the adhesive layer,[2] including the effects of strain rate,[3–5] fatigue,[6–8] and mode mixity.[9–11] One of the adhesive material parameters required for CZM is the critical energy release rate. Thus, several methods have been proposed and standardized to measure the energy release rate (ERR).[12–15] ERR is also known to be strain rate dependent[16–21] Therefore, tests should be performed under various loading conditions to evaluate the strain rate dependence of ERR.

Under static loading conditions, a double cantilever beam (DCB) test method was developed to measure the mode I critical energy release rate, G_{IC}, of the adhesive joints.[13,14] Here, we refer to this as the standard DCB test. The ERR calculation using simple beam theory (SBT) or Timoshenko beam theory requires experimental measurements of the load, opening displacement, and crack length. However, optical crack length measurements contain uncertainties. Therefore, digital image correlation and mechanoluminescence are suggested for crack position determination.[22,23] Besides the challenges related to crack length measurement, the effective crack length is affected by the fracture process zone and root rotation. Therefore, crack length correction[24,25] and the compliance method[26] have been proposed to account for these effects in the effective crack length. Crack length correction is conducted by plotting one-third of the compliance versus the measured crack; this is called the corrected beam theory (CBT). Correction factors for the end block and large displacement were also introduced in the CBT.[27,28] The compliance method is a data reduction technique that uses beam theory to replace crack length with load and displacement and is called the compliance-based beam method (CBBM).[26] The ERR can also be calculated by differentiating the compliance with respect to the crack length, which is called the experimental compliance method (ECM). The J-integral approach was used to calculate the fracture energies in the DCB tests from a different perspective.[29–33] This approach requires measurements of the load and rotation angle at the load point.

Under dynamic loading conditions, the test methods significantly influenced the results of the DCB tests. In the standard DCB test method, increasing the loading rate leads to an asymmetric fracture as movement occurs only on one side of the loading point due to the effect of inertia, as shown in Figure 1a, resulting in mixed-mode fractures.[18] To address this issue, a freefall wedge was employed to open a DCB specimen symmetrically under dynamic loading conditions, as shown in Figure 1b.[20, 34–37] This method involves pushing a wedge in the same direction as the crack growth. A guided double-cantilever beam test method is also proposed for dynamic DCB tests.[38] In this method, the wedge is pulled in the opposite direction of crack growth. Regardless of the direction of wedge insertion, using the wedge to open the DCB specimen results in symmetric deformations in the adherends, which is advantageous, particularly under dynamic loading conditions.

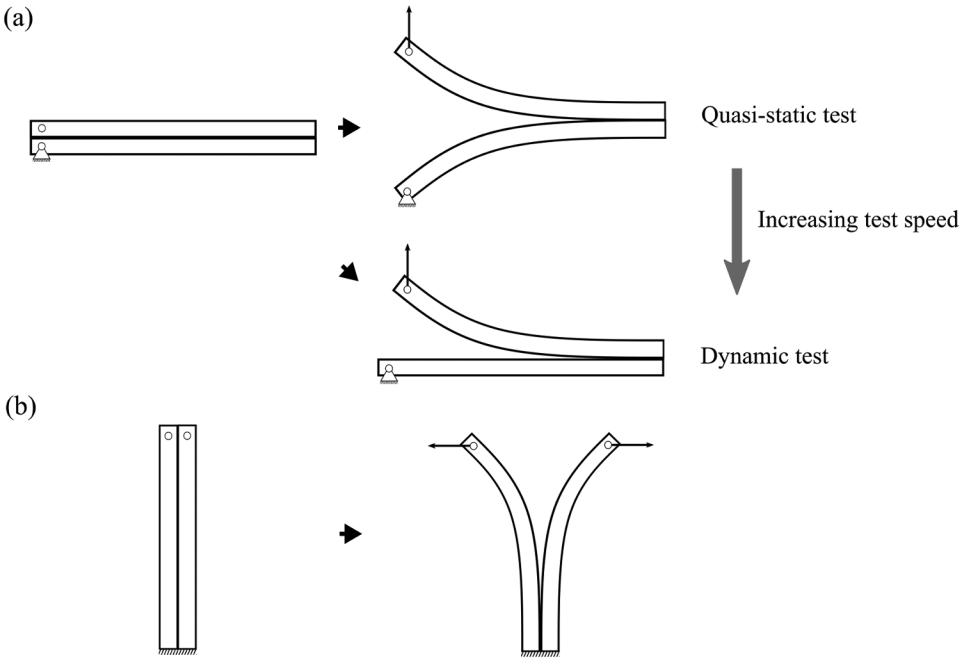

Figure 1. Schematics of the beam deformation under (a) Asymmetric opening and (b) Symmetric opening.

However, the direction of the load applied to the ends of the specimens differs from that in the standard test method. For the standard DCB tests, only the load vertical to the longitudinal direction of the specimen was applied; thus, the moment at the crack front was expressed as the product of the crack length and load. Conversely, when the wedge was used to open the DCB specimen, the axial load was also applied, resulting in an additional moment related to beam deflection. Thus, it is important to discuss the effect of the axial load on the ERR for different wedge angles. Because the sign of the additional moment changes depending on the direction of wedge insertion, theoretical discussions were conducted separately.

First, we introduce the theory of driving a wedge in the direction of crack growth, that is, the wedge-inserted DCB (WDCB) method. Thorsson et al.[36] introduced a correction factor that accounted for the effect of the moment caused by the axial load acting on a pin block, which was limited to right-angled wedges. Oshima et al.[39] considered the effect of an additional bending moment generated by an axial load and a pin block on the ERR for arbitrary wedge angles. Zarifpour et al.[37] considered the effect of shear deformation on the strain energy using the Timoshenko beam theory, in addition to the additional moment due to the pin blocks. However, as the deformation increases, the opening displacement cannot be ignored compared with the distance of the load point shift by the pin block. Therefore, the additional

moment formed by the product of the axial load and opening displacement must be considered[40]; however, no closed-form solution has been proposed for the WDCB thus far.

Next, we introduce the theory of pulling a wedge in the direction opposite to the crack growth, that is, guided DCB (GDCB). The relationship between the load, opening displacement, and crack length in a simple beam subjected to normal and axial end forces was approximated by Awtar et al.,[41] summarized by Liu and Yan,[42] and applied by Medina et al.[30] to calculate the ERR of the GDCB in the approximate solution. Although the discussion of GDCB has been limited to right-angled wedges, this method has a great potential to be extended to the discussion of the arbitral wedge angle, including opposite wedge insertion.

The primary objective of this study is to establish an accurate calculation method for fracture energy in wedge-opening DCB tests. First, the ERR for wedge-opening DCB tests are investigated with arbitrary wedge angles. The J-integral method is investigated by considering the load in the longitudinal direction. Next, a numerical analysis is conducted with varying wedge angles to compare the load, crack length, and displacement results and examine the accuracy of the proposed method. Finally, the pin-block effect on the fracture energy is discussed.

2. Theory

2.1. ERR Calculation

In the standard DCB test, a load was applied at the end of the beam in a direction normal to the longitudinal direction of the specimen, as shown in Figure 2. Using SBT, the relation between the load P, opening displacement δ, and crack length a is given as

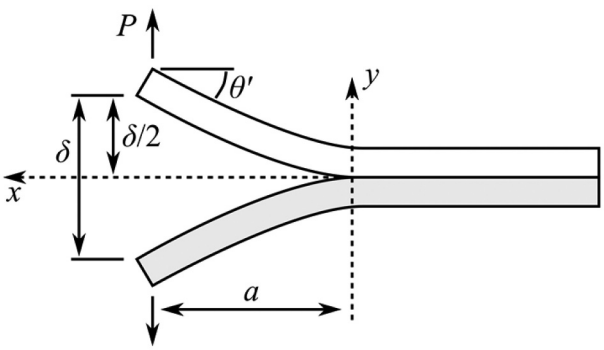

Figure 2. Standard double-cantilever beam test configuration.

$$\frac{\delta}{P} = \frac{2a^3}{3EI}, \tag{1}$$

where E is the Young's modulus of the substrate. I is the moment of inertia of the substrate given by $I = bh^3/12$, where h and b denote the thickness and width of the substrate. According to linear elastic fracture mechanics, the energy release rate G of the cracked substrate is given as a function of the moments at the crack front[28,43] as

$$G = \frac{8M_1^2 + 8M_2^2 - (M_1 + M_2)^2}{16bEI}, \tag{2}$$

where M_1 and M_2 are the moments at the crack fronts of the upper and lower substrates, respectively. Because the standard DCB test yields

$$M_{(x=0)} = M_1 = -M_2 = Pa, \tag{3}$$

the ERR is derived as

$$G = \frac{P^2a^2}{bEI} = \frac{9EI\delta^2}{4ba^4}. \tag{4}$$

In contrast to the standard test methods, several methods for propagating cracks in DCB specimens using tools have been proposed, as shown in Figure 3. In these methods, the longitudinal movement of the angled tool generates symmetric deformation of the beams, which is an advantage, particularly when testing at high speeds. However, the wedge applies a load that is not vertical in the longitudinal direction, resulting in an additional moment at the crack front. Therefore, the effect of axial load on the ERR must be considered.

Here, a wedge angle is denoted as $2|\theta|$, where the wedge faces away from the crack growth direction for $\theta > 0$ and opposite for $\theta < 0$, as shown in Figure 3. When $\theta > 0$, the load, crack length and displacement are given as shown in Figure 4. The moment acting on the beam is given by

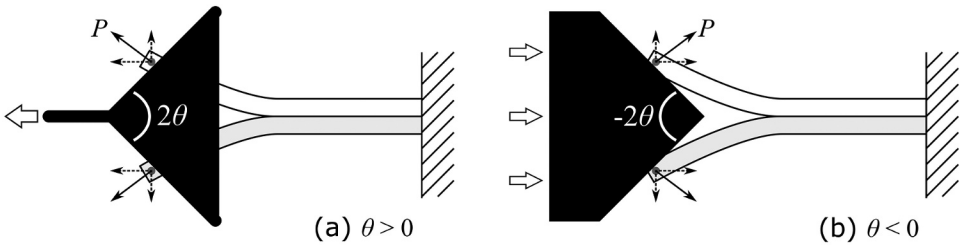

Figure 3. Schematics of wedge-opening double-cantilever beam test for (a) $\theta > 0$ and (b) $\theta < 0$.

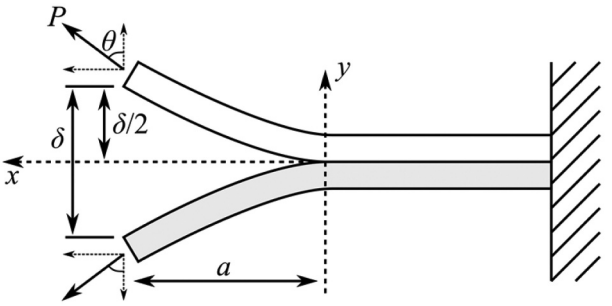

Figure 4. Wedge-opening double-cantilever beam test configuration.

$$M_{(x)} = -P\cos\theta(a-x) + P\sin\theta\left(\frac{\delta}{2} - y\right), \tag{5}$$

where the moment is the function of x and the deformation in the longitudinal direction was assumed to be negligible. Therefore, ERR is obtained as follows:

$$G = \frac{M_{(x=0)}^2}{bEI} = \frac{P^2a^2\cos^2\theta}{bEI}\left(1 - \frac{\delta}{2a}\tan\theta\right)^2. \tag{6}$$

However, ERR is expressed as a function of three parameters: load, displacement, and crack length. Conversely, the simple beam theory yields the deflection of the beam as

$$\frac{d^2y}{dx^2} = -\frac{M_{(x)}}{EI}. \tag{7}$$

Substituting Eq. (5) in Eq. (7) and solving the differential equations, the moment at the crack front can be expressed as follows:

$$M_{(0)} = -\frac{P\cos\theta}{\alpha}\tanh\alpha a, \tag{8}$$

where $\alpha = \sqrt{P\sin\theta/EI}$. Thus, ERR was obtained as a function of load and crack length:

$$G = \frac{P\cos\theta}{b\tan\theta}\tanh^2\alpha a. \tag{9}$$

In addition, the relationship between the load, opening displacement, and crack length is given as

$$\delta = \frac{2}{\alpha\tan\theta}(\alpha a - \tanh\alpha a). \tag{10}$$

Therefore, two of the three parameters must be measured to calculate the ERR in wedge-opening DCB tests.

When the wedge is pushed toward crack growth to open the specimen, the wedge angle is considered negative ($\theta < 0$). In this case, by given $\alpha' = i\alpha = \sqrt{-P\sin\theta/EI}$, Eqs. (9) and (10) can be re-expressed as

$$G = -\frac{P\cos\theta}{b\tan\theta}\tan^2\alpha' a; \tag{11}$$

$$\delta = \frac{2}{\alpha'\tan\theta}(-\alpha' a + \tan\alpha' a). \tag{12}$$

2.2. J integral method

The J integral for homogeneous linear and nonlinear elastic material in a two-dimensional deformation field is defined as

$$J = \int_{\Gamma}\left(W\mathrm{d}y - \boldsymbol{T}\cdot\frac{\partial \boldsymbol{u}}{\partial x}\mathrm{d}s\right), \tag{13}$$

where $W, \boldsymbol{T}, \boldsymbol{u}$, and $\mathrm{d}s$ denote the strain energy density, traction vector, displacement vector, and element length along the outer path Γ, respectively. For standard DCB tests, the J integral is obtained as:

$$J = \frac{2P}{b}\sin\theta' \approx \frac{2P}{b}\theta', \tag{14}$$

where θ' is the rotation angle at the beam edge (see Figure 2).[30] In this case, the integral path is set inside the adherend. Therefore, if the adherend does not undergo plastic deformation, the J integral matches the ERR, that is $J = G$. For wedge-opening DCB tests, the traction consists of axial and normal components when choosing the outer surface of the specimen as the integration path in the same manner as Paris and Paris.[29] Therefore, the J-integral is given as

$$J = \int_{\Gamma}\left(T_{xy}\frac{\partial u}{\partial x}\mathrm{d}x + T_{yy}\frac{\partial v}{\partial x}\mathrm{d}x\right). \tag{15}$$

The contribution to the integral is zero everywhere on this integral path except at the load points. Due to the rotation of the beam end, dx of the load point changes by $du = (1-\cos\theta')dx$ in the x-direction and $dv = \sin\theta' dx$ in the y-direction from the undeformed state, as shown in Figure 5.[40] At the load point, $P\sin\theta$ in the x-direction and $P\cos\theta$ in the y-direction are applied when the rotation angle of the beam end reaches θ'. Therefore, in the case of $\theta = -45°$,

$$J = \frac{2P'}{B}(\sin\theta' + 1 - \cos\theta'), \tag{16}$$

is given, where $P' = -P\sin\theta = P\cos\theta$.[40] Modifying Eq. (16) to arbitrary wedge angles,

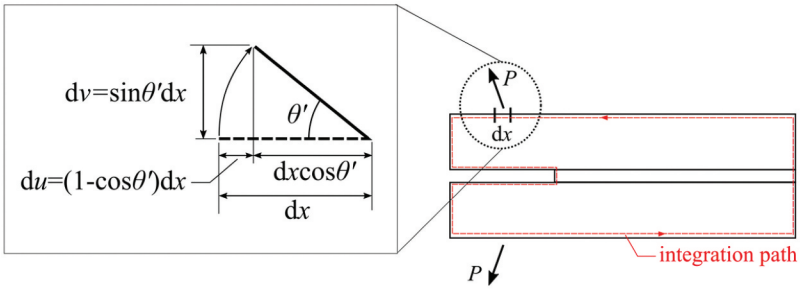

Figure 5. *x* and *y* components of the unit tangent vector at a load point.

$$J = \frac{2P\cos\theta}{b}\sin\theta' - \frac{2P\sin\theta}{b}(1-\cos\theta') \tag{17}$$

is obtained.

3. Numerical analysis

A numerical analysis was conducted to evaluate the accuracy of the theoretical fracture energy evaluation of wedge-opening DCB tests. A finite element model of the wedge-opening DCB tests was created using a pre/postprocessor (LS-PrePost 4.11) and analyzed using the explicit method in Ansys LS-DYNA (ver. R9.1.0), which is suitable for solving nonlinear processes with large deformations and complex contact problems. The dimensions of the DCB specimen were 200 mm length, 25 mm width, and 0.1 mm adhesive thickness with a pre-crack length of 30 mm (see Figure 6). Three adherend thicknesses, $h = 2,\ 5,\ and\ 10$ mm, were used to investigate the effect of bending stiffness, and $h = 2$ mm was used to investigate the wedge angle effect. A half model was used to reduce the computing resources. The ends of the specimen were constrained for all translations and rotations.

The adherends were modeled as elastic bodies, with $E = 210\ GPa\ and\ \nu = 0.3$, and formulated as one-integration-point solid elements. The minimum and maximum mesh sizes of the adherend were 0.3125 and 2.5 mm, respectively, as shown in Figure 7. Loading pins, with a diameter of 1.5 mm, made of a rigid body were attached to the side of the adherend. The loading wedge, with tip angles 2θ from −150° to 150°, was modeled with the same material as the loading pins. The friction between the loading pin and wedge was assumed to be zero.

The adhesive was formulated as an 8-noded 4-integration point cohesive element and had the following parameters with reference to general epoxy adhesives: $E = 3711$ MPa, $\nu = 0.36$, tensile yield stress $T = 20$ MPa, and mode I energy release rate $G_{IC} = 500$ J/m^2. A cohesive zone model with a triangular traction separation law (MAT240 in LS-DYNA) was used to analyze the adhesive layer.

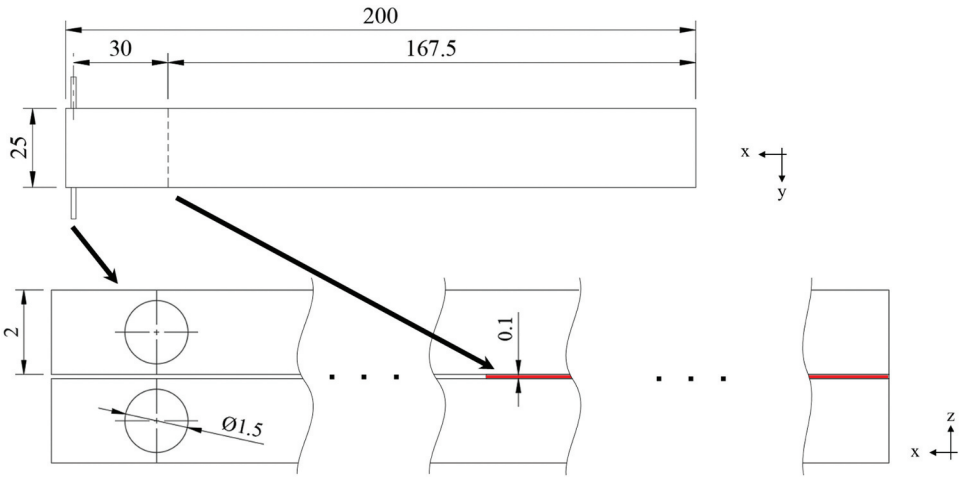

Figure 6. Dimensions of the DCB specimen with 2-mm thickness adherend.

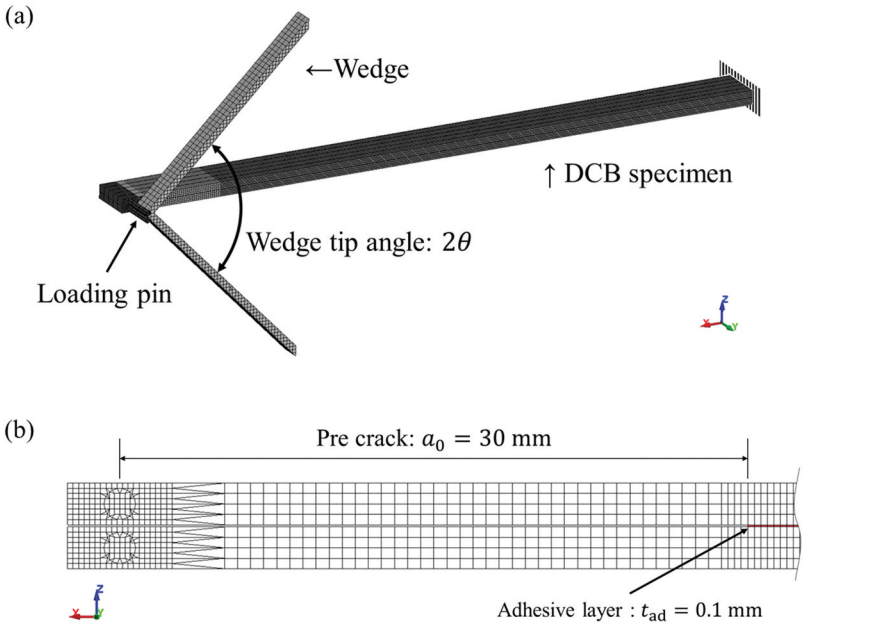

Figure 7. (a) Finite element model overview and (b) Finite element mesh of the specimen.

4. Results and discussion

4.1. Theoretical and numerical analysis

For a given ERR and load, the crack length can be obtained by applying Newton's method to Eq. (9) for $\theta > 0$ and Eq. (11) for $\theta < 0$. The relationship between the normal load $P\cos\theta$ and opening displacement for a constant ERR was obtained, as shown in Figure 7a. Furthermore, by applying these results to

Eq. (10) for $\theta > 0$ and Eq. (12) for $\theta < 0$, the relationship between the crack length and opening displacement was obtained, as shown in Figure 8b. In the wedge-opening DCB tests, an additional moment due to the axial load was generated compared with the standard DCB tests, and its impact increased as the wedge angle became more obtuse or the opening displacement increased. In particular, the larger the wedge angle, the larger the load, and the faster the crack propagation at the same displacement.

Figure 9 compares the theoretical and numerical results of the relationship between the load and displacement in the wedge-opening DCB tests for three different wedge angles. For both positive and negative wedge angles, the load – opening displacement curves of the theoretical and numerical analyses showed good agreement, even at large wedge angles. The theoretical model considered the moments generated by the normal and longitudinal loads but ignored the longitudinal deformation of the beam. Conversely, the numerical model considered both. Therefore, the effect of the longitudinal deformation was negligible. In addition, a theoretical model that considers additional moments can be applied to a wide range of wedge angles.

In the case of the wedge angle $|2\theta| = 150°$, the crack propagation stopped and the load started to oscillate after a certain opening displacement (see Figure 9c). When crack stagnation occurred, the internal strain energy calculated in the numerical analysis suddenly decreased and subsequently increased, as shown in Figure 10. A similar phenomenon was observed even for small wedge angles when the cracks propagated sufficiently. This is because the shorter crack length increased the likelihood of bending deformation. However, the situation changed once the cracks propagated. The bending deformation of the beam was released, resulting in a complex stress state in the beam, as shown in Figure 11. Consequently, the crack propagation stopped.

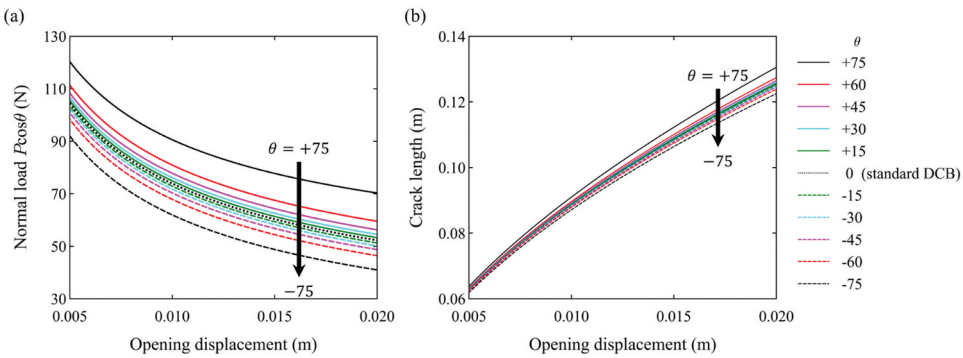

Figure 8. (a) Load – displacement relationship and (b) Crack length – displacement relationship varying wedge angles in the case of $G = 500$ J/m^2, $h = 2$ mm, $b = 25$ mm, and $E = 210$ GPa.

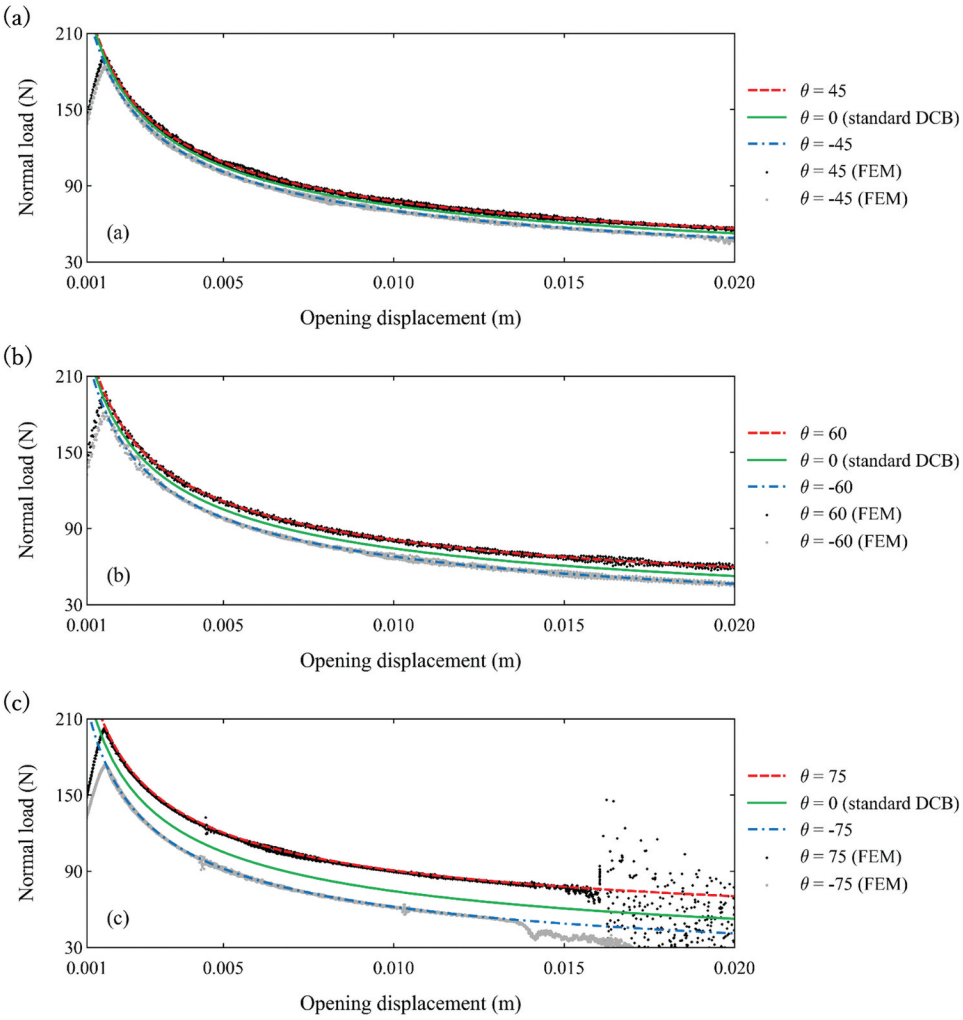

Figure 9. Relationship between the load and displacement in the case of $G = 500$ J/m^2, $h = 2$ mm, $b = 25$ mm, and $E = 210$ GPa for (a) $\theta = \pm 45°$, (b) $\theta = \pm 60°$, and (c) $\theta = \pm 75°$.

4.2. Effects of the additional moment due to axial load

By introducing a theoretical model that considers the additional moment, the change in the relationship between the normal load, displacement, and crack length from the standard DCB case was derived in the previous section. Conversely, this section discusses the effect of the additional moment on the ERR by comparing these theories with and without an additional moment. A calculation error arises when applying the theoretical model neglecting the additional moment (that is, the model for the standard DCB) to calculate the ERR of the wedge-opening DCB tests. This error indicates the magnitude of the additional moment effect.

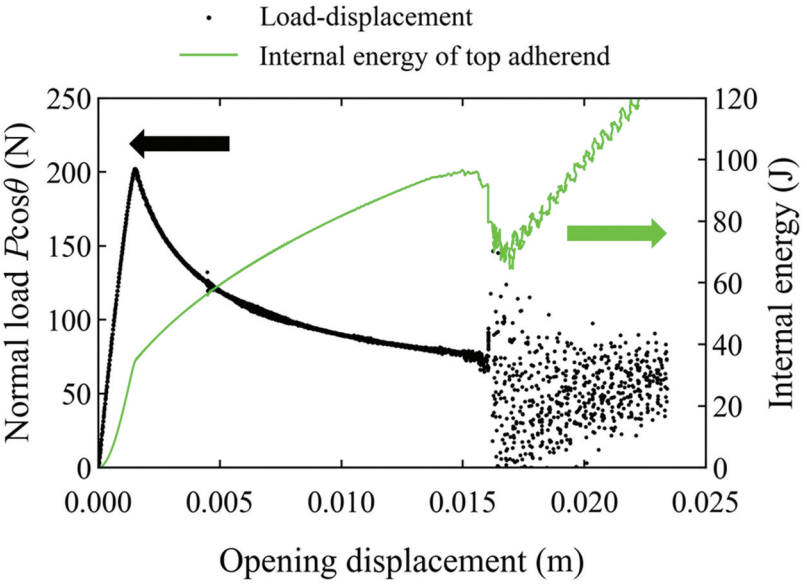

Figure 10. Load and internal energy against opening displacement for $\theta = 75°$.

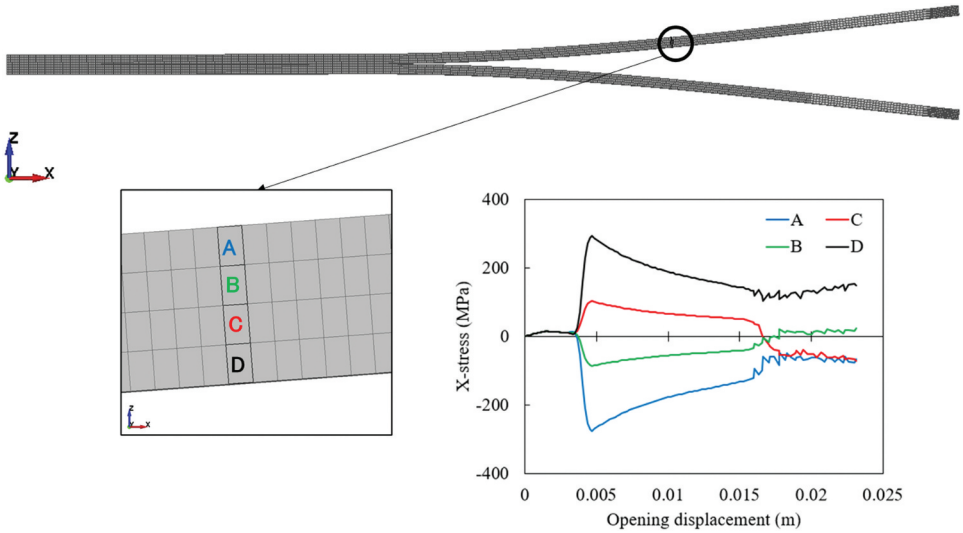

Figure 11. The stress-displacement curve in the thickness direction of the adherend at a certain position.

First, the specimen geometry and ERR of the adhesive were determined, and the load – displacement relationship was obtained using the numerical analysis of the wedge-opening DCB tests. The ERR was then back-calculated using the standard DCB test method. The difference between the input and calculated ERR represents the calculation error due to an additional moment. Figure 12 shows the calculated ERR, neglecting the additional moment when

the input ERR was 500 J/m^2. The load in the longitudinal direction increased with the obtuse wedge angle, and the opening displacement increased with the crack length. Because the additional moment is expressed as the product of the load in the longitudinal direction and the opening displacement, the more obtuse the wedge and the greater the displacement, the greater is the additional moment effect. The error value between the input and calculated ERR is defined as

$$\text{Error}(\%) = \frac{G_{\text{cal}} - G_{\text{input}}}{G_{\text{input}}} \times 100, \tag{18}$$

where G_{cal} is the back-calculated ERR, and G_{input} is the input ERR. ERR in the plateau region of the R-curve was averaged and used for error evaluation. Figure 13 shows the error variation with respect to the wedge angle for $G_{\text{input}} = 500$ J/m^2 and an adherend thickness of 2 mm. Back-calculation of ERR using the method that considers the additional moment was also conducted to check the validity of the proposed model. For $\theta = 15$ degrees, the errors were negligibly small enough, even when neglecting the additional moment effect. In addition, the error remained small over a wide range of wedge angles when the proposed model was used. However, the error increased to 5% or more with wedge angles above 90 degrees for the model without additional moments. Because 90-degree wedges are often used to equalize horizontal and vertical loads,[36–40] caution is required when discussing ERR at such large wedge angles. For $\theta > 0$, neglecting the axial load effect

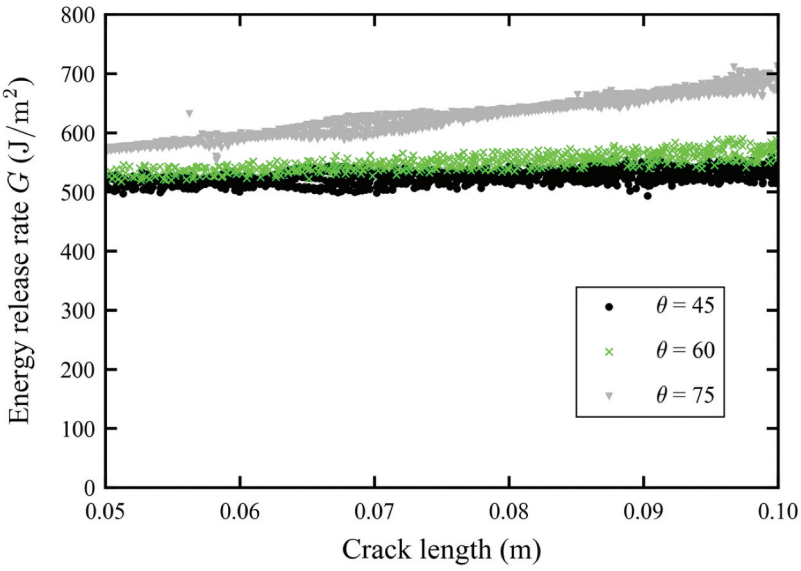

Figure 12. Back-calculated energy release rate using the standard DCB test method for $\theta = 45$, 60, and 75°.

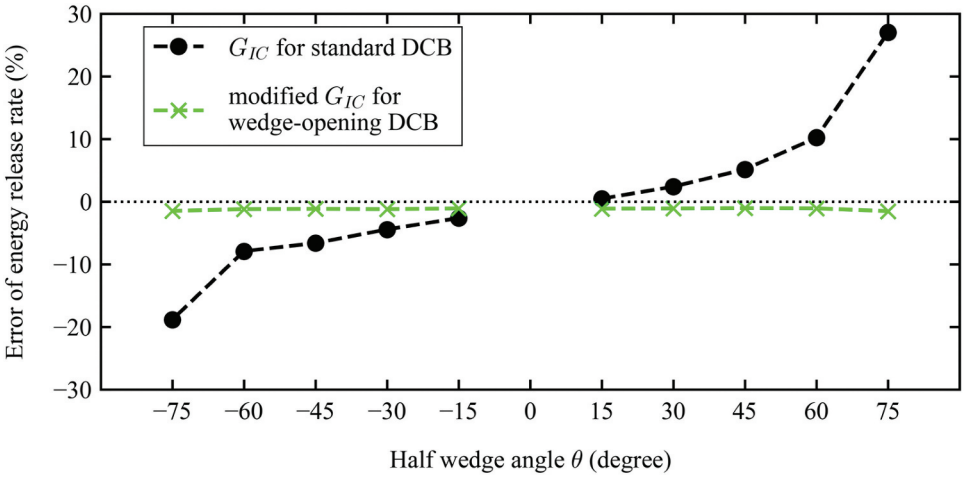

Figure 13. Error in the energy release rate calculation against half-wedge angles in the case of $G_{IC} = 500$ J/m^2 and $h = 2$ mm.

leads to overestimating the ERR, whereas the opposite is true for $\theta < 0$. In Figure 14, the effect of adherend thickness was shown in the case of $G_{input} = 500$ J/m^2 and the wedge angle $\theta = 45$. The thicker the adherend, the smaller the additional moment effect. Figure 15 shows the comparison of $G_{input} = 500$ J/m^2 and 1500 J/m^2 with the same adherend geometry for the adherend thickness of 2 mm and $\theta > 0$. For the same adherend thickness, an increase in ERR leads to an increase in the load and deformation, resulting in an increase in the additional moment. Thus, the error increases with a larger ERR when the additional moment effect is neglected. Increasing the adherend thickness is effective in reducing the error when the ERR is large, but the proposed ERR method can sufficiently reduce the error even when the ERR is large and the adherend is thin.

4.3. Pin block effect

Pin blocks are commonly used in DCB tests, especially for thin adherends; however, the load point shifts, necessitating compensation (Figure 16). Displacement correction using an end-block correction factor, N, was applied for standard DCB tests.[13,24] In the case of the wedge-opening DCB tests, the moment and displacement were affected by the pin block. In particular, the additional moment effect owing to the load point shift was significant. However, modifying Eq. (5) to account for the additional moment from the pin block makes the differential equation unsolvable, preventing ERR determination.

The ERR calculation was affected by the moment at the crack front. Therefore, several models have been proposed from the perspective of

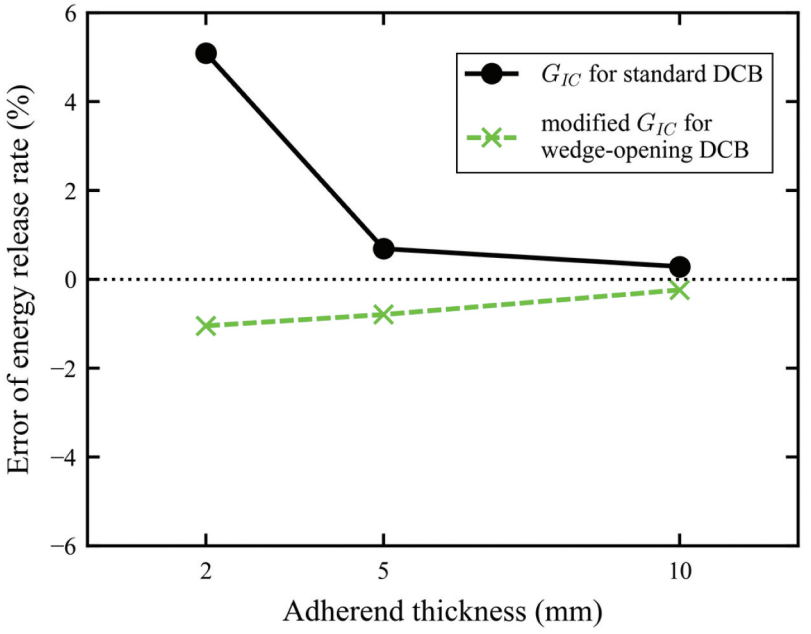

Figure 14. Error in the energy release rate calculation against adherend thickness in the case of $G_{IC} = 500$ J/m^2 and $\theta = 45°$.

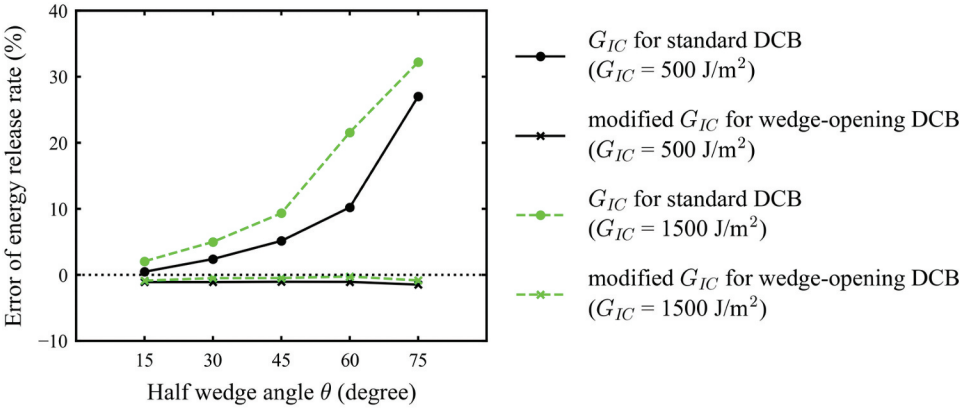

Figure 15. Error in the energy release rate calculation with a critical energy release rate of G_{IC} =500 and 1500 J/m^2 for $\theta > 0°$.

moment correction owing to the load point shift by introducing bin blocks.[36,37,39,40] However, a solution that considers both the pin block and large deformation effects has not yet been proposed. Conversely, the J integral approach is not affected by the pin block effect because the rotation angle of the beam edge, rather than the moment, is used to calculate the fracture energy. To verify the applicability of the J-integral approach, the pin block effect was evaluated by back-calculating the fracture energy using finite

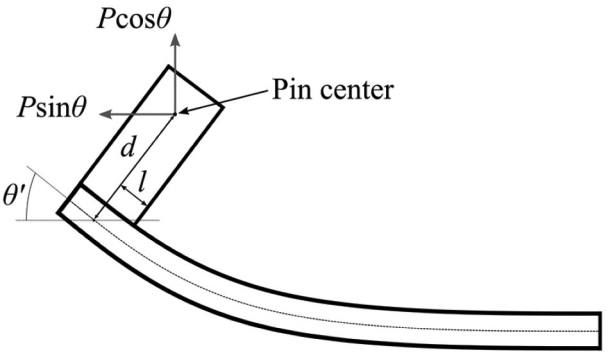

Figure 16. Schematic of the pin block for the DCB specimen.

element analysis. The pin block, with a distance of load point shift $d = 6$ mm and a half width $l = 2.5$ mm, was modeled using the same material as the adherend, as shown in Figure 17. The model with an adherend thickness $h = 2$ mm and a half-wedge angle $\theta = \pm 45$ degrees was used. The rotation angle of pin blocks was determined by calculating the slope between points on the block. Eq. (4), (9), (11), (14), and (17) were used for the fracture toughness calculation, and Eq. (18) was used to calculate the error. The error values are shown in Figure 18. Without a pin block, the errors in Eq. (4), (9), and (11) were less than 2% (see Figure 14); however, with the pin block, the errors increased to more than 5%. Conversely, for the modified J-integral approach, the error in the fracture energy was less than 2% even when the pin block was installed. Therefore using the modified J approach appears to be the most promising method for calculating the fracture toughness in wedge-opening DCB tests when pin blocks are employed.

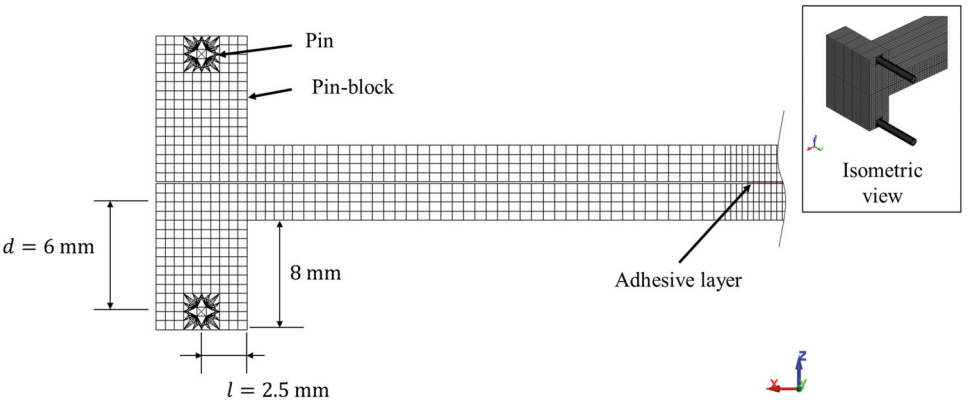

Figure 17. Finite element model with pin block.

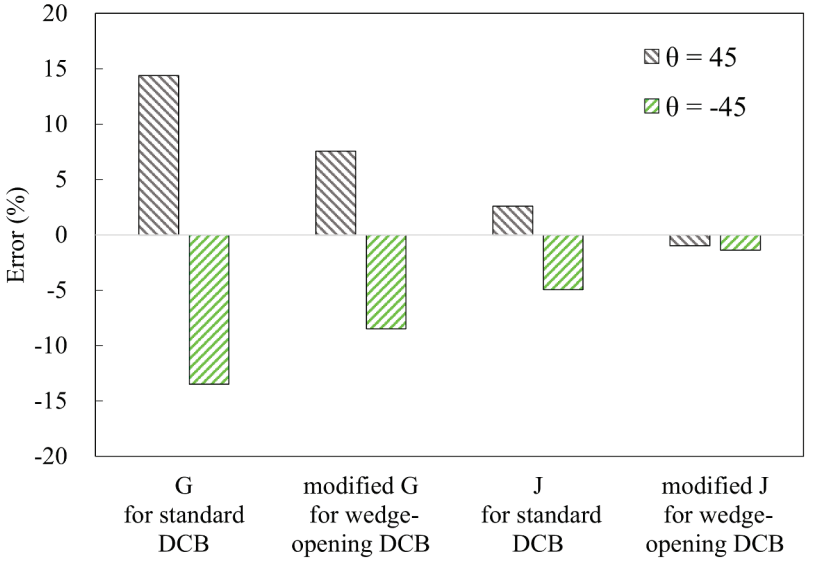

Figure 18. Error in the fracture energy calculations when the pin block is installed.

5. Conclusion

The fracture energy calculation for the wedge-opening DCB test method was performed from two perspectives. First, the energy release rate is discussed. This approach required two of the three experimentally measurable parameters (load, displacement, and crack length) for the calculation. A calculation method was proposed to consider the additional moment owing to the axial load for any wedge angle. Although the energy release rate calculation for the standard DCB test can be applied with a low error if the wedge angle is sufficiently small and the adherend is sufficiently thick, the proposed method, specific to the wedge-opening DCB test method, yields more accurate results. Next, we discussed the J-integral approach, which requires a load and rotation angle at the beam edge. This method was modified to consider additional moments. Although this approach requires the measurement of the angle at the beam end instead of displacement, the modified J-integral method emerged as a promising approach when pin blocks are employed. Experiments are often limited to measurable parameters, limiting the choice of calculation methods. Therefore, it is crucial to select a method with minimal error from the available experiments; the results presented here will help in making this decision.

Disclosure statement

No potential conflict of interest was reported by the author(s).

References

[1] Adams, R. D. *Adhesive Bonding: Science, Technology and Applications*; Woodhead Publishing Limited: UK, 2005.

[2] Alfano, M.; Furgiuele, F.; Leonardi, A.; Maletta, C.; Paulino, G. H. Cohesive Zone Modeling of Mode I Fracture in Adhesive Bonded Joints. *Key Eng. Mater.* 2007, *348-349*, 13–16. DOI: 10.4028/www.scientific.net/KEM.348-349.13.

[3] Marzi, S.; Hesebeck, O.; Brede, M.; Kleiner, F. A Rate-Dependent Cohesive Zone Model for Adhesively Bonded Joints Loaded in Mode I. *J. Adhes. Sci. Technol.* 2009, *23*(6), 881–898. DOI: 10.1163/156856109X411238.

[4] Jia, Z.; Yuan, G.; Feng, X.; Zou, Y. Numerical Study on the Mechanical Behavior of a Polyurethane Adhesive Under High Strain Rate. *Compos. B Eng.* 2019, *158*, 131–140. DOI: 10.1016/j.compositesb.2018.08.110.

[5] Valente, J. P. A.; Campilho, R. D. S. G.; Marques, E. A. S.; Machado, J. J. M.; da Silva, L. F. M. Geometrical Optimization of Adhesive Joints Under Tensile Impact Loads using Cohesive Zone Modelling. *Int. J. Adhes. Adhes.* 2020, *97*, 102492. DOI: 10.1016/j.ijadhadh.2019.102492.

[6] Khoramishad, H.; Crocombe, A. D.; Katnam, K. B.; Ashcroft, I. A. Predicting Fatigue Damage in Adhesively Bonded Joints Using a Cohesive Zone Model. *Int. J. Fatigue* 2010, *32*(7), 1146–1158. DOI: 10.1016/j.ijfatigue.2009.12.013.

[7] de Moura, M. F. S. F.; Gonçalves, J. P. M. Cohesive Zone Model for High-Cycle Fatigue of Adhesively Bonded Joints Under Mode I Loading. *Int. J. Solids Struct.* 2014, *51*(5), 1123–1131. DOI: 10.1016/j.ijsolstr.2013.12.009.

[8] Costa, M.; Viana, G.; Créac'Hcadec, R.; da Silva, L. F. M.; Campilho, R. D. S. G. A Cohesive Zone Element for Mode I Modelling of Adhesives Degraded by Humidity and Fatigue. *Int. J. Fatigue* 2018, *112*, 173–182. DOI: 10.1016/j.ijfatigue.2018.03.014.

[9] Floros, I. S.; Tserpes, K. I.; Löbel, T. Mode-I, Mode-II and Mixed-Mode I+II Fracture Behavior of Composite Bonded Joints: Experimental Characterization and Numerical Simulation. *Compos. B Eng.* 2015, *78*, 459–468. DOI: 10.1016/j.compositesb.2015.04.006.

[10] Rocha, A. V. M.; Akhavan-Safar, A.; Carbas, R.; Marques, E. A. S.; Goyal, R.; El-Zein, M.; Da Silva, L. F. M. Numerical Analysis of Mixed-Mode Fatigue Crack Growth of Adhesive Joints Using CZM. *Theor. Appl. Fract. Mech.* 2020, *106*, 102493. DOI: 10.1016/j.tafmec.2020.102493.

[11] Yang, Z.; Xia, Y.; Yang, F.; Zhu, Z.; Sun, Y.; Jiang, H. Peeling Angle Effect on Soft Adhesive: Mixed-Mode CZM Considering Fibrillation. *Eng. Fract. Mech.* 2022, *274*, 108778. DOI: 10.1016/j.engfracmech.2022.108778.

[12] ISO 15024. Fibre-Reinforced Plastic Composites – Determination of Mode I Interlaminar Fracture Toughness, GIC, for Unidirectionally Reinforced Materials. *ISO Stand.* 2011.

[13] ISO 25217. Adhesives –Determination of the Mode 1 Adhesive Fracture Energy of Structural Adhesive Joints using Double Cantilever Beam and Tapered Double Cantilever Beam Specimens. *ISO Stand.* 2009.

[14] ASTM D3433-99. *Standard Test Method for Fracture Strength in Cleavage of Adhesives in Bonded Metal Joints*. American Society for Testing and Materials, West Conshohocken, 2012.

[15] ASTM D5528. *Standard Test Method for Mode I Interlaminar Fracture Toughness of Unidirectional Fiber-Reinforced Polymer Matrix Composites 1*. American Society for Testing and Materials, West Conshohocken, 2007.

[16] Kin Loch, A. J.; Shaw, S. J. The Fracture Resistance of a Toughened Epoxy Adhesive. *J. Adhes.* 1981, *12*(1), 59–77. DOI: 10.1080/00218468108071189.

[17] Blackman, B. R. K.; Dear, J. P.; Kinloch, A. J.; Macgillivray, H.; Wang, Y.; Williams, J. G.; Yayla, P. The Failure of Fibre Composites and Adhesively Bonded Fibre Composites Under High Rates of Test. *J. Mater. Sci.* 1995, *30*(23), 5885–5900. DOI: 10.1007/BF01151502.

[18] Blackman, B. R. K.; Kinloch, A. J.; Rodriguez Sanchez, F. S.; Teo, W. S.; Williams, J. G. The Fracture Behaviour of Structural Adhesives Under High Rates of Testing. *Eng. Fract. Mech.* 2009, *76*(18), 2868–2889. DOI: 10.1016/j.engfracmech.2009.07.013.

[19] Blackman, B. R. K.; Kinloch, A. J.; Rodriguez-Sanchez, F. S.; Teo, W. S. The Fracture Behaviour of Adhesively-Bonded Composite Joints: Effects of Rate of Test and Mode of Loading. *Int. J. Solids Struct.* 2012, *49*(13), 1434–1452. DOI: 10.1016/j.ijsolstr.2012.02.022.

[20] Sekiguchi, Y.; Yamagata, Y.; Sato, C. Mode I Fracture Energy of Adhesive Joints Bonded with Adhesives with Different Characteristics Under Quasi-Static and Impact Loading. *J. Adhes. Soc. Jpn.* 2017, *53*, 330–337. DOI: 10.11618/adhesion.53.330.

[21] Sekiguchi, Y.; Sato, C. Experimental Investigation of the Effects of Adhesive Thickness on the Fracture Behavior of Structural Acrylic Adhesive Joints Under Various Loading Rates. *Int. J. Adhes. Adhes.* 2021, *105*, 102782. DOI: 10.1016/j.ijadhadh.2020.102782.

[22] Sun, F.; Blackman, B. R. K. Using Digital Image Correlation to Automate the Measurement of Crack Length and Fracture Energy in the Mode I Testing of Structural Adhesive Joints. *Eng. Fract. Mech.* 2021, *255*, 107957. DOI: 10.1016/j.engfracmech.2021.107957.

[23] Terasaki, N.; Fujio, Y.; Sakata, Y.; Horiuchi, S.; Akiyama, H. Visualization of Crack Propagation for Assisting Double Cantilever Beam Test Through Mechanoluminescence. *J. Adhes.* 2018, *94*(11), 867–879. DOI: 10.1080/00218464.2018.1423968.

[24] Williams, J. G. End Corrections for Orthotropic DCB Specimens. *Compos. Sci. Technol.* 1989, *35*(4), 367–376. DOI: 10.1016/0266-3538(89)90058-4.

[25] Hashemi, S.; Kinloch, A. J.; Williams, J. The Analysis of Interlaminar Fracture in Uniaxial Fibre-Polymer Composites. *Proc. R. Soc. Lond. A.* 1990, *427*, 173–199. DOI: 10.1098/rspa.1990.0007.

[26] de Moura, M. F. S. F.; Morais, J. J. L.; Dourado, N. A New Data Reduction Scheme for Mode I Wood Fracture Characterization Using the Double Cantilever Beam Test. *Eng. Fract. Mech.* 2008, *75*(13), 3852–3865. DOI: 10.1016/j.engfracmech.2008.02.006.

[27] Williams, J. G. Large Displacement and End Block Effects in the 'DCB' Interlaminar Test in Modes I and II. *J. Compos. Mater.* 1987a, *21*(4), 330–347. DOI: 10.1177/002199838702100403.

[28] Williams, J. G. Large Displacement Effects in the DCB Test for Interlaminar Fracture in Modes I and II. *Proc. ICCM ECCM* ISBN: 185166114x, 9781851661145 1987b, *3*, 233–242.

[29] Paris, A. J.; Paris, P. C. Instantaneous Evaluation of J and C. *Int. J. Fract.* 1988, *38*(1), R19–R21. DOI: 10.1007/BF00034281.

[30] Andersson, T.; Stigh, U. The Stress–Elongation Relation for an Adhesive Layer Loaded in Peel Using Equilibrium of Energetic Forces. *Int. J. Solids Struct.* 2004, *41*(2), 413–434. DOI: 10.1016/j.ijsolstr.2003.09.039.

[31] Ji, G.; Ouyang, Z.; Li, G.; Ibekwe, S.; Pang, S.-S. Effects of Adhesive Thickness on Global and Local Mode-I Interfacial Fracture of Bonded Joints. *Int. J. Solids Struct.* 2010, *47*(18–19), 2445–2458. DOI: 10.1016/j.ijsolstr.2010.05.006.

[32] Sun, F.; Blackman, B. R. K. A DIC Method to Determine the Mode I Energy Release Rate G, the J-Integral and the Traction-Separation Law Simultaneously for Adhesive Joints. *Eng. Fract. Mech.* 2020, *234*, 107097. DOI: 10.1016/j.engfracmech.2020.107097.

[33] Granja, D. M.; Simões, B.; Carbas, R.; Marques, E.; da Silva, L. F. M. Establishment of the Cohesive Law of an Epoxy Adhesive Using the Direct Method and the Effect of the

Substrate Material. *J. Mech. Solids* 2022, *1*(1), 15–24. DOI: 10.24840/2975-8262_001-001_001836.

[34] Xu, S.; Dillard, D. A. Determining the Impact Resistance of Electrically Conductive Adhesives Using a Falling Wedge Test. *IEEE Trans. Compon. Packag. Technol.* 2003, *26* (3), 554–562. DOI: 10.1109/tcapt.2003.817646.

[35] Yamagata, Y.; Lu, X.; Sekiguchi, Y.; Sato, C. Experimental Investigation of Mode I Fracture Energy of Adhesively Bonded Joints Under Impact Loading Conditions. *Appl. Adhes. Sci.* 2017, *5*(1). DOI: 10.1186/s40563-017-0087-7.

[36] Thorsson, S. I.; Waas, A. M.; Schaefer, J.; Justusson, B.; Liguore, S. L. Effects of Elevated Loading Rates on Mode I Fracture of Composite Laminates using a Modified Wedge-Insert Fracture Method. *Compos. Sci. Technol.* 2018, *156*, 39–47. DOI: 10.1016/j.compscitech.2017.12.018.

[37] Zarifpour, D.; Khoramishad, H.; Marzbanrad, J. Dynamic Fracture Response of Adhesive Joints Subjected to Mode-I Impact Wedge Loading. *J. Adhes.* 2024, *100*(15), 1442–1459. DOI: 10.1080/00218464.2024.2317219.

[38] Medina, S. A.; González, E. V.; Blanco, N.; Pernas-Sánchez, J.; Artero-Guerrero, J. A. Guided Double Cantilever Beam Test Method for Intermediate and High Loading Rates in Composites. *Int. J. Solids Struct.* 2023, *264*, 112118. DOI: 10.1016/j.ijsolstr.2023.112118.

[39] Oshima, S.; Yoshimura, A.; Hirano, Y.; Ogasawara, T. Experimental Method for Mode I Fracture Toughness of Composite Laminates Using Wedge Loaded Double Cantilever Beam Specimens. *Compos. A.* 2018, *112*, 119–125. DOI: 10.1016/j.compositesa.2018.05.036.

[40] Ding, J. C.; Xu, W. Determination of Mode I Interlaminar Fracture Toughness of Composite by a Wedge-Insert Double Cantilever Beam and the Nonlinear J Integral. *Compos. Sci. Technol.* 2021, *206*, 108674. DOI: 10.1016/j.compscitech.2021.108674.

[41] Awtar, S.; Slocum, A. H.; Sevincer, E. Characteristics of Beam-Based Flexure Modules. *J. Mech. Des.* 2007, *129*(6), 625–639. DOI: 10.1115/1.2717231.

[42] Liu, P.; Yan, P. A Modified Pseudo-Rigid-Body Modeling Approach for Compliant Mechanisms with Fixed-Guided Beam Flexures. *Mech. Sci.* 2017, *8*(2), 359–368. DOI: 10.5194/ms-8-359-2017.

[43] Williams, J. G. On the Calculation of Energy Release Rates for Cracked Laminates. *Int. J. Fract.* 1988, *36*(2), 101–119. DOI: 10.1007/BF00017790.